

# A Platform to Study the Effects of Electrical Stimulation on Immune Cell Activation During Wound Healing

Kaiping Wang, Udit Parekh, Jonathan K. Ting, Natasha A. D. Yamamoto, Juan Zhu, Todd Costantini, Ana Claudia Arias, Brian P. Eliceiri,\* and Tse Nga Ng\*

Wound healing is a complex process involving diverse changes in multiple cell types where the application of electric fields has been shown to accelerate wound closure. To define the efficacy of therapies based on electric fields, it would be valuable to have a platform to systematically study the effects of electrical stimulation (ES) upon the inflammation phase and the activation of signaling mediators. Here, an *in vivo* ES model in which flexible electrodes are applied to an animal model for monitoring inflammation in a wound is reported on. Subcutaneous implants of polyvinyl alcohol sponges elicit inflammation response as defined by the infiltration of leukocytes. The wound site is subjected to electric fields using two types of additively fabricated flexible electrode arrays. The sponges are then harvested for flow cytometry analysis to identify changes in the phosphorylation state of intracellular targets. This platform enables studies of molecular mechanisms, as it shows that an application of low-frequency ES  $\leq 0.5$  Hz increases phosphorylation of Erk proteins in recruited leukocytes, identifying a signaling pathway that is activated during the healing process.

Acute and chronic wounds are a significant healthcare burden, and technologies for wound management<sup>[1–3]</sup> are highly desired. Since the endogenous electric field at wound sites is a critical driver of the healing process,<sup>[4,5]</sup> electrical stimulation (ES) of wound sites has been proposed as a means to accelerate the wound healing process and supplement the standard of care.<sup>[6–9]</sup> ES is thought to reduce the chances of infection, increase angiogenesis, and accelerate cell migration. The effects of ES on cutaneous wound healing in animal<sup>[10]</sup> as well

as clinical studies<sup>[6,8,11]</sup> have demonstrated that there is an unmet need for standardized platforms to assess the efficacy of specific parameters in wound healing. Here, we focus on the inflammation phase. While *in vitro* studies have demonstrated the effects of electric fields on cell migration and dissected parts of the molecular machinery driving these effects,<sup>[12–14]</sup> *in vivo* studies have focused primarily on large scale changes like wound area and angiogenesis.<sup>[7,8]</sup> *In vivo* studies to gain insights into the molecular mechanisms of these effects have been limited, and a platform for uncovering the complex interactions driven by ES *in vivo* would be a valuable complementary tool to gain further mechanistic insights into the inflammation component of the wound healing process.


Here, we report a platform that enables sensitive *in vivo* studies of changes in protein levels upon ES at wound sites on mice. The platform consisted of a polyvinyl alcohol (PVA) sponge which was implanted subcutaneously at the wound site. Instead of tissue extraction, this PVA sponge enabled the capture and investigation of infiltrating immune cells.<sup>[15–18]</sup> Using subcutaneous implants of PVA sponges, we are able to establish data in animal models that can be measured in a laboratory setting. Such PVA sponges could be used as subcutaneous implants in humans with appropriate controls in a clinical setting.<sup>[19]</sup> The additively printed<sup>[20,21]</sup> ES electrodes used in this study were flexible with enhanced adhesion to skin, allowed precise control over stimulation locations, and were optimized for improved charge injection capacity.<sup>[22,23]</sup> As prior meta-studies<sup>[6,8,11]</sup> show that there is ongoing debate over the types of ES parameters necessary for wound treatment, the magnitude and frequency of ES waveforms were varied here to examine their effects on immune cells in mice wound models.

To assess the effects of ES, the cells captured in the PVA sponge were analyzed via flow cytometry, which enabled high-throughput measurement of cell populations and intra-cellular protein levels at the single cell level.<sup>[24]</sup> The multi-parametric flow cytometry analysis allowed us to isolate signals from specific sub-populations of cells, to rapidly distinguish different cell types in particular immune cells and investigate cell-type-specific signal transduction pathways.

K. Wang, U. Parekh, Prof. T. N. Ng  
Department of Electrical and Computer Engineering  
University of California San Diego  
9500 Gilman Drive, La Jolla, CA 92093, USA  
E-mail: tnn046@ucsd.edu

Prof. T. Costantini, Prof. B. P. Eliceiri  
Department of Surgery  
University of California San Diego  
USA  
E-mail: beliceiri@ucsd.edu

J. K. Ting, N. A. D. Yamamoto, Dr. J. Zhu, Prof. A. C. Arias  
Department of Electrical Engineering and Computer Sciences  
University of California Berkeley  
253 Cory Hall, Berkeley, CA 94720, USA

 The ORCID identification number(s) for the author(s) of this article can be found under <https://doi.org/10.1002/adbi.201900106>.

DOI: 10.1002/adbi.201900106

We demonstrate the versatility of the platform by investigating markers for two different signaling pathways that mediate immune cell response to ES, specifically phosphorylation-driven signaling events. Phosphorylation plays a key role in regulating protein activities and plays an important role in driving signaling cascades<sup>[25]</sup> which guide cellular response to external stimuli. We focus on the Mapk (mitogen activated protein kinases)/Erk (extracellular signal-regulated kinases) and PI3k (phosphatidylinositol 3-kinase)/Akt (protein kinase B) pathways, which are known to play roles in immune cell activation and development,<sup>[26–31]</sup> and also known to play a role in cell migration during wound healing.<sup>[13,30]</sup>

As shown in **Figure 1A**, the wound model was created on the dorsal region of a 6- to 8-week-old male C57BL/6 mouse. Following the subcutaneous implantation of PVA sponges into the mice, they were maintained in an unstimulated state, without electrodes attached, to enable the normal leukocyte infiltration for 3 days after sponge implantation as previously described.<sup>[15]</sup> Afterward, mice were electrically stimulated with constant-current square-wave pulses for 1 h at varying currents and frequencies (Figure 1B,C). The stimulation current range was chosen based on previous studies applying electrical stimulation to wound areas in animal models and patients.<sup>[6,10]</sup> We chose to apply a monophasic current stimulation, hypothesizing that applying an exogenous electric field in the same direction as the wound field<sup>[4]</sup> would maximize the effect of stimulation. The pulsed nature of the applied field would minimize heating effects from long application of constant direct current and potential electrochemical effects in the vicinity of the electrodes at the skin–electrode interfaces.<sup>[32–34]</sup>

The ES electrodes used in this study were additively printed to integrate the wires for easy placement and precise control of stimulation over different wound regions. Two types of electrodes in **Figure 2** were fabricated and tested to demonstrate applicability across different electrode geometries and substrate characteristics, as well as to demonstrate applicability with high-density electrodes which can be used for spatial mapping. Specifically, we used a low-density, stretchable array fabricated

on a substrate with strong adhesion characteristics via facile screen printing, and a high-density array fabricated via inkjet printing, suitable for impedance mapping.

The screen-printed array in **Figure 2A** was fabricated on a stretchable substrate made of the silicone elastomer polydimethylsiloxane (PDMS), into which a small amount of ethoxylated polyethylenimine (PEIE) was added. This addition of PEIE has been shown to modify the PDMS cross-linking network to increase stretchability and van der Waals adhesion by introducing microscale wrinkles on the elastomer surface,<sup>[20,35]</sup> thus serving as a good substrate for devices which need to adhere to skin. The electrodes consisted of a central electrode and four equally spaced outer electrodes, as shown in **Figure 2B**. During stimulation, the central electrode was placed on the wound site while the outer electrodes were on the unwounded tissue. This configuration allowed an electric field to be directed from inside to outside the wound area or vice versa. The interconnects were patterned by blade-coating Ag/AgCl ink mixed with a stretchable elastomer (Ecoflex),<sup>[20]</sup> yielding stretchable traces as shown in **Figure S1**, Supporting Information, with high conductivity of 2000 S/cm to enable low-impedance connections between the electrodes and controller hardware.

The inkjet-printed array in **Figure 2C** was fabricated on a flexible polyethylene naphthalate substrate by printing gold interconnects using a gold nanoparticle ink.<sup>[21]</sup> The traces were insulated by attaching a Teflon tape on top, with vias in the tape having been cut by a laser-cutter. The finer patterning capability of the inkjet printing process allows for rapid prototyping and fabrication of high-density arrays. We demonstrated the capability of these arrays to map areas of varying impedance, as found in wound areas which would have lower impedance in regions with damaged skin compared to undamaged skin. We used hydrogel phantoms to create areas of low and high impedance and measured the impedance magnitude and phase angle between pairs of neighboring electrodes. Measurements of the impedance angle distinguish the regions of low and high conductivity as discussed in ref. [3] and shown in **Figure 2D**.

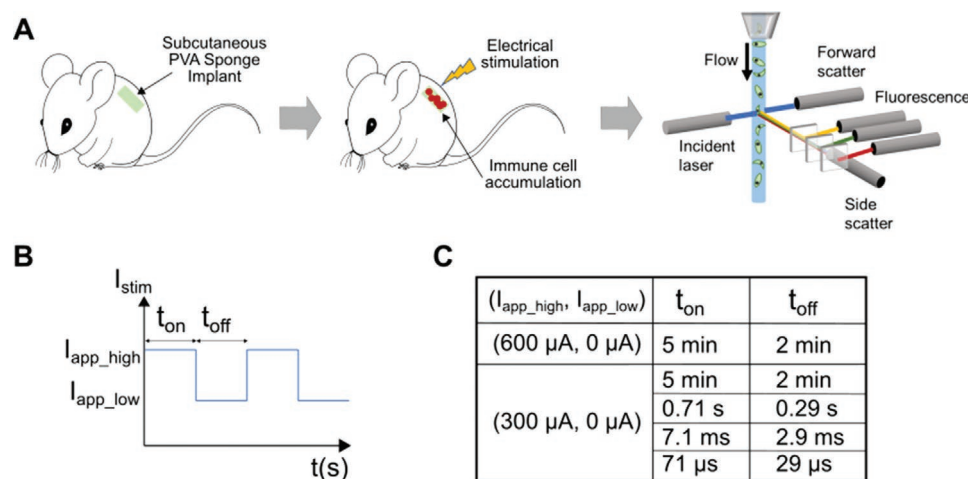


**Figure 1.** A) Schematic of the experimental workflow. Cells infiltrated in the sponge are harvested for analysis by flow cytometry. B) Schematic of the stimulation waveform. C) Table listing the stimulation parameters.

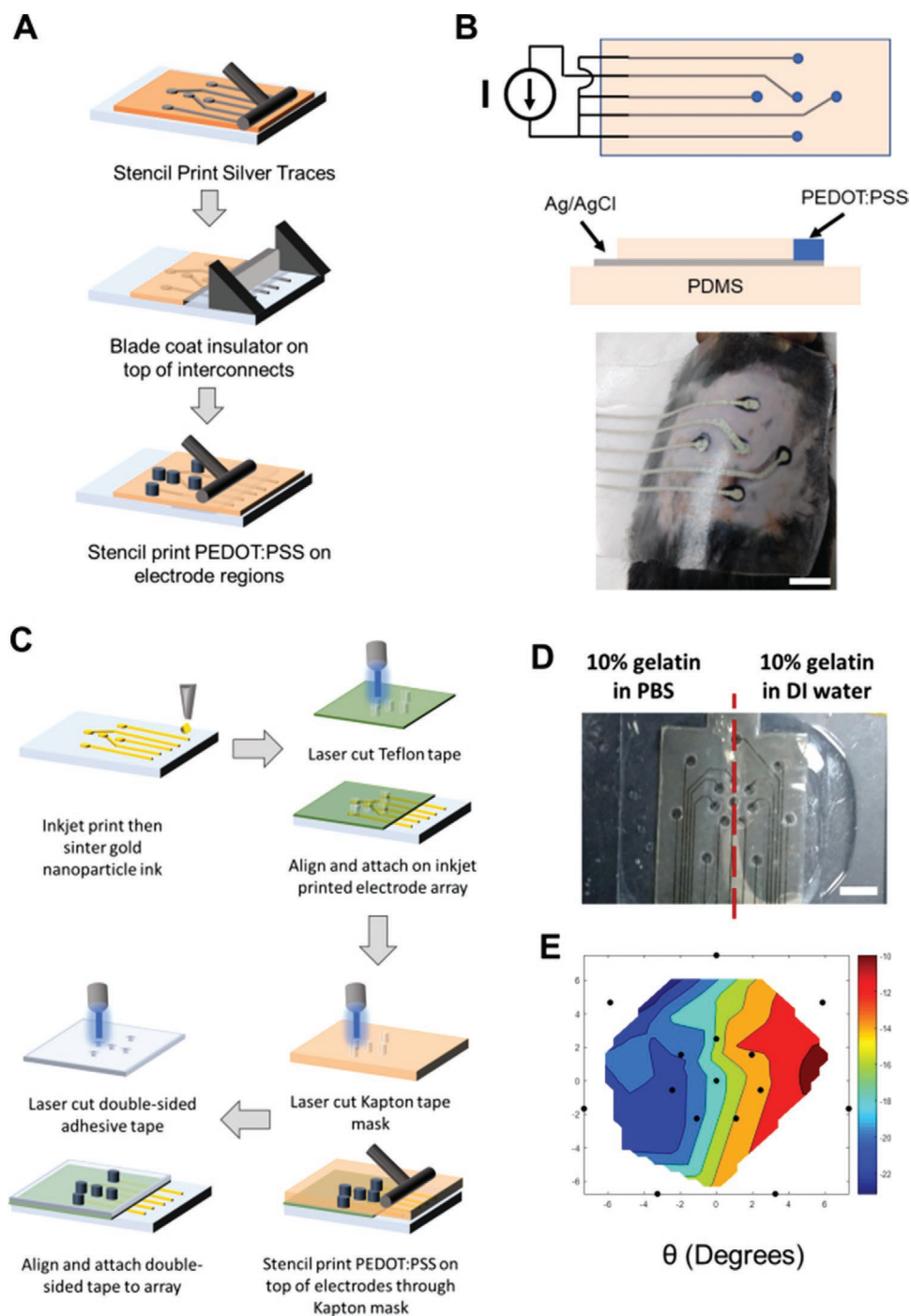


**Figure 2.** A) Fabrication process of screen-printed electrodes. B) Schematic of the stimulation setup and photograph of electrodes mounted on top of the wound site, where the implanted sponge was beneath the center electrode. Scale bar: 9 mm. C) Fabrication process for inkjet-printed electrodes. D) Demonstration of impedance mapping using inkjet-printed electrodes on hydrogel phantoms. Scale bar: 5 mm. E) Spatial maps of impedance magnitude and angle between pairs of neighboring electrodes. Black dots indicate electrode location.

Both screen-printed and inkjet-printed electrodes were covered with a conducting polymer poly(3,4-ethylenedioxythiophene) polystyrene sulfonate (PEDOT:PSS) to provide a stable, biocompatible interface,<sup>[20,36–39]</sup> to further lower the impedance at the electrode-skin interface, and to provide a greater charge injection capacity for ES than metal surfaces.<sup>[22,23]</sup> As shown

in Figure S2, Supporting Information, the electrodes without PEDOT:PSS coated on the ends exhibited a reduction in current supplied over time, reducing from 300  $\mu\text{A}$  to less than 10  $\mu\text{A}$  current after 40 min, while the PEDOT:PSS-coated electrodes maintained the current magnitude for the full 1 h stimulation time. The electrode arrays with PEDOT:PSS were then used in

our ES studies comparing the effects of applied current amplitudes and frequencies, as shown in the table of Figure 1C. The ES power supply was in constant-current mode, and voltage was monitored to limit the voltage to a maximum of 5 V.

To determine whether ES would have any deleterious effect on cell viability, we assessed the fraction of live cells at the applied current magnitudes of 300 and 600  $\mu\text{A}$  for 1 h. The applied square waveform frequency was at 2.3 mHz (a period of 7 min, with 5 min on to 2 min off for each duty cycle as detailed in Figure 1C), and only current magnitudes were varied. After stimulation, the PVA sponges were extracted from the wound site, and cells were harvested from the sponge. A subset of the harvested cells was treated with the stain propidium iodide, which selectively enters and labels only dead cells due to their greater membrane permeability. The treated sample was analyzed using flow cytometry. The single-cell population was obtained by gating the single-cell region of forward- and side-scatter signals in Figure 3A. In this single-cell subset, viable cells were ones not permeated by the propidium iodide dye and were counted within the indicated region of interest. The percentage of viable cells was calculated as given in Figure 3B, with no significant differences in viability observed between ES applied at 300  $\mu\text{A}$ , 600  $\mu\text{A}$ , and sham. We also conducted

an upper bound experiment by stimulating the wound for 3 days at 600  $\mu\text{A}$ , 2.3 mHz for 1 h per day (diamond symbols in Figure 3B) and found that the fraction of viable cells is comparable to the sham condition.

To demonstrate the applicability of the platform to study cell types that are characteristic of the inflammatory phase of wound healing, and more physiologically relevant compared to in vitro systems, we chose to focus on CD45<sup>+</sup> infiltrating leukocytes cells. As the viability was determined to be unaffected by ES, a subset of the harvested cells were fixed, permeabilized, and labeled with fluorescently tagged antibodies against the pan-leukocyte surface marker CD45, phosphorylated Erk, or phosphorylated Akt to assess which pathways were activated in infiltrating immune cells upon application of ES. The phosphorylation of Erk was determined based on the role of the Mapk/Erk signaling cascade regulating the response to extracellular stimuli such as growth factors and extracellular matrix that mediate cellular responses including proliferation, activation, differentiation, and survival.<sup>[28]</sup> Phosphorylation of Akt was determined based on its role in the PI3k/Akt signaling network in regulating cell survival, angiogenesis, chemotaxis, activation, and maturation.<sup>[29]</sup> The labeled cells were analyzed by the process detailed in Figure 4A.

Using the same waveform as the above viability evaluation, we examined the effect of varying current magnitudes on phosphorylation of Erk and Akt using site specific antibodies to each target in permeabilized CD45<sup>+</sup> cells. Following flow cytometry, single cells were gated, and within this subset the CD45<sup>+</sup> population was gated for further analysis. Here, the stain CD45 was used to identify inflammatory leukocytes, since it is a pan-leukocyte marker,<sup>[40]</sup> and thus capturing the Erk or Akt signal across multiple CD45<sup>+</sup> cell types. CD45<sup>+</sup> cells were assessed for phosphorylated Erk (P-Erk) or Akt (P-Akt) fluorescence intensity, as shown in Figure 4A. To study whether ES effects were driven by factors specific to the electrode geometry or materials, we conducted ES experiments with both the screen-printed and inkjet-printed electrodes (Figure S3, Supporting Information). With the inkjet-printed array, the electric field between the wound site and the intact tissue were at a slightly higher magnitude (1 V mm<sup>-1</sup>) as compared to the experiments with screen-printed electrodes (0.83 V mm<sup>-1</sup>).

We observed in Figure 4B that ES at both 300 and 600  $\mu\text{A}$  increased P-Erk compared to the sham controls. Thus, we used the 300  $\mu\text{A}$  current to be safely within the viability and effective ES range in the subsequent experiments. As such, we also found that the increase in P-Erk level was comparable regardless of electrode density.

Next, we tested whether the frequency of stimulation could modulate the response of the Erk pathway, since the frequency dependence of signaling pathway activation has been observed previously in vitro.<sup>[41,42]</sup> The frequency of the square wave pulse was varied over six orders of magnitude to discern the frequency dependence of Erk or Akt phosphorylation. P-Erk levels were observed to be increased over sham at low ES frequencies, 2.3 mHz and 0.5 Hz, while no significant effect was observed for ES at the higher frequencies tested in Figure 4C. In contrast, P-Akt levels were unaffected by the application of ES across all the frequency range tested in Figure 4D, thus indicating that the Erk pathway is among the earliest signaling

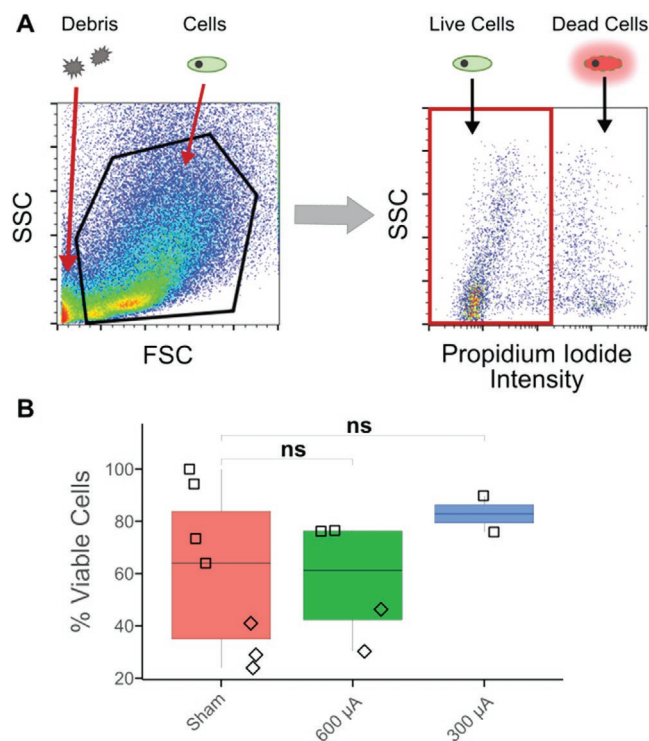


**Figure 3.** Effect of stimulation current magnitudes on cell viability. A) Flow cytometry analysis workflow. Gating region for scattered light signals from single cells (left), and for fluorescence signal from dead cells by propidium iodide viability stain (right). SSC is the signal from side-scattered light and FSC is the signal from forward-scattered light. B) Comparison of viability for different applied current magnitudes versus sham. The stimulation was at 2.3 mHz for 1 h, with □ representing 1-day experiments, and ◇ representing three consecutive days of applying stimulation or sham condition. “ns” indicates not significant  $p$ -value  $> 0.05$ .

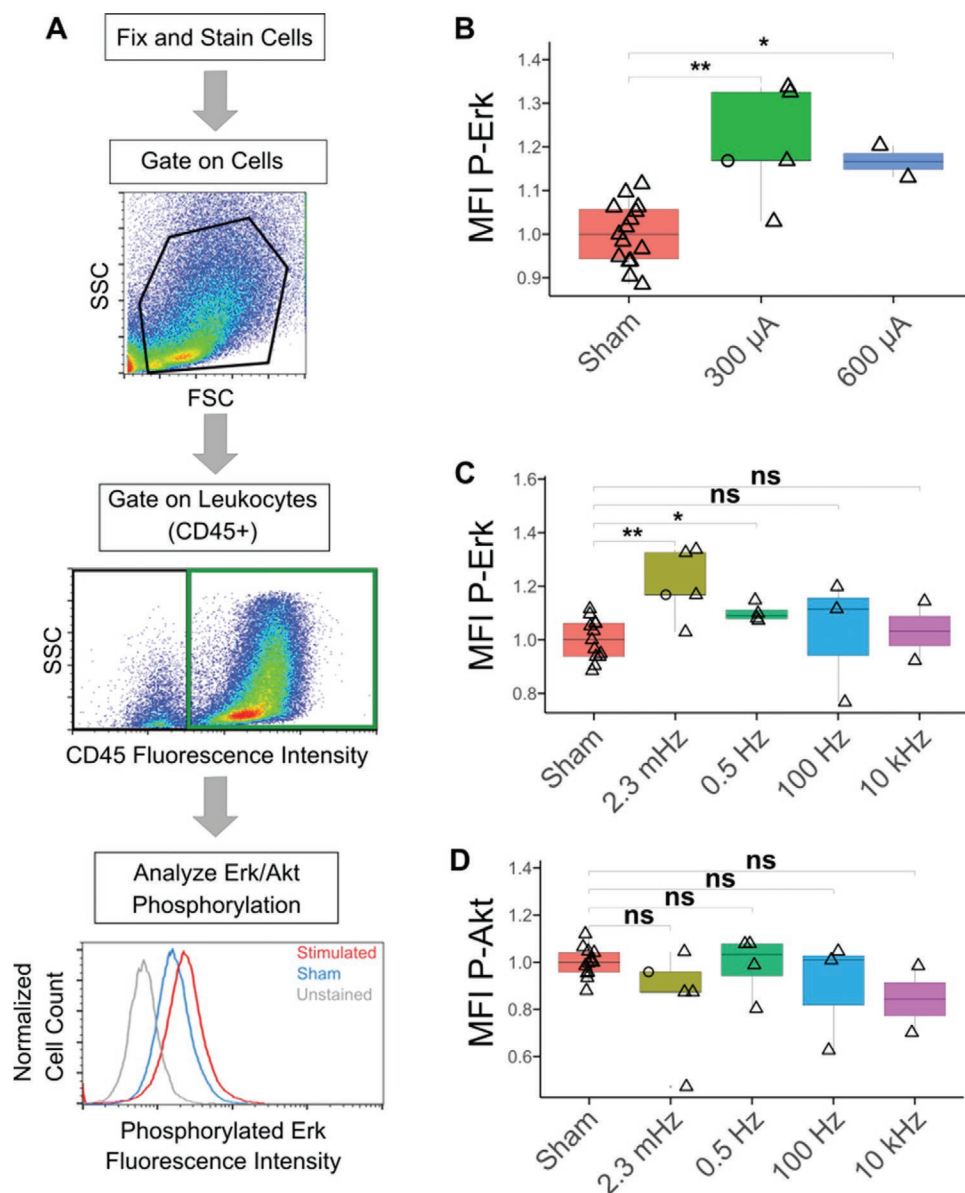


**Figure 4.** Electrical stimulation–driven activation in immune cells. A) Flow cytometry gating and signal measurement workflow. Gating regions for scattered light signal from cells, CD45+ stained cells, and representative histograms of phosphorylated Erk signals. B) Mean fluorescence intensity (MFI) of Erk phosphorylation in CD45+ cells, for different applied current  $\leq 0.5$  Hz. C) MFI of Erk phosphorylation and D) MFI of Akt phosphorylation in CD45+ cells. (C) and (D) are carried out under an applied current of 300  $\mu$ A amplitude. Data points represented by o are for experiments conducted with inkjet printed electrodes; data points represented by  $\Delta$  are for experiments conducted with screen-printed electrodes. \* indicating  $p$ -value  $\leq 0.05$ , and \*\* indicating  $p$ -value  $\leq 0.01$ . “ns” indicates not significant  $p$ -value  $> 0.05$ .

pathways involved in the transduction of electrical signals in immune cells. The increase in P-Erk levels at 2.3 mHz low-frequency stimulation was consistent across both electrode densities tested. The results show that Erk pathway activation is preferred over Akt after electrical stimulation and demonstrates feasibility to study intracellular changes based on our platform.

While in vitro studies have indicated the activation of various signaling pathways upon ES, in vivo effects have been more difficult to measure. The platform developed in this report is a step toward enabling systematic mechanistic in vivo studies

on specific cell types. We determined that Erk phosphorylation was part of the early response of inflammatory cells to ES in sterile PVA sponge implants. We also showed that Erk activation is a frequency-dependent phenomenon and was absent at frequencies above 100 Hz. Meta-studies<sup>[6,8]</sup> of clinical studies using ES found that a wide range of ES conditions including high-frequency pulses were used. Our results showed that the high-frequency waveforms  $>100$  Hz would not be effective for increasing Erk phosphorylation events in CD45+ cells. This frequency dependence may be due to the polarization time

of intra-cellular proteins, which may be unable to follow the applied electric field as the frequency was increased. We note that this frequency dependence may be different for other cell types,<sup>[41,42]</sup> which may respond to higher frequencies based on their biological function, and for different settings such as during *in vitro* assays.

In our approach, we achieved multi-parametric quantification of protein changes at the single cell level. The increase in ERK phosphorylation might be due to different levels of ERK activities in various cell types or in different phases of the same cell type. There is the possibility that ERK activation occurs in certain sub-types rather than increase the activation in all leukocytes. Future work will investigate the subsets of leukocytes to hone in on the origin of increased ERK activation. In the future, we may also conduct multiplexed analysis along with flow cytometry, such as assaying changes in extra-cellular factors like cytokines and growth factors to further study signaling pathways for wound healing. The activation of one pathway may cross-inhibit the other signaling cascade, or may cross-activate substrates present in the other network. Thus, Erk activation may lead to inhibition of Akt activation or activation of downstream Akt substrates without Akt phosphorylation.<sup>[31]</sup> The differential activation of the pathways<sup>[29–31,43]</sup> governing cell survival, differentiation, and activation would be useful for understanding the healing process.

On the other hand, we also note certain limitations in this subcutaneous platform.<sup>[15–18]</sup> To extend the PVA model to other types of surface wound such as open wounds or ulcers, the rate of cell infiltration, cell viability, contamination, impedance, and variability of the injury site would need to be taken into account. Nonetheless, with optimization, the PVA sponge implants can be readily applied to other mouse backgrounds and testing of other ES strategies. While the presence of the PVA sponge is by definition a foreign body response, there is the potential for full-thickness skin wounds to have different leukocyte responses to ES. Future ES studies could be done with an open wound with the goal of defining the effect of ES on the normal versus chronic wound healing processes.

Our ES procedure utilizes flexible electrodes that are easy to fabricate, provide convenient control over stimulation locations, and the additive manufacturing processes used allow rapid prototyping and testing. The conformal form factor and roughened surface to enhance adhesion aids our electrode arrays to remain in place on curved body surfaces. Thus, these electrode arrays can enable low-cost, disposable, easily applicable bandages for short stimulation sessions.

Taken together, the PVA sponge implant model to define the inflammation component of wound healing, combined with stretchable electrode arrays, offers a versatile platform to examine the effects of ES parameters on molecular mechanisms that occur during the wound healing process. This approach provides molecular readouts relevant in leukocytes that can be readily expandable to other pathways using the range of available and well-characterized phosphorylation state-specific antibodies. We observed that the Erk pathway is activated in inflammatory leukocytes when low-frequency electrical stimulation  $\leq 0.5$  Hz is applied at the wound site. In contrast, the Akt pathway was not affected by ES application.

Future studies may be directed toward identifying the different signaling pathways in sub-populations of cells that are activated during the healing process, thus helping to build a comprehensive map of cell-type-specific signal transduction networks driving wound healing. Such a map could then be harnessed to develop advanced solutions to accelerate wound healing.

## Experimental Section

**Screen-Printed Electrode Fabrication:** Electrodes were fabricated as detailed in ref. [20]. The substrate was polydimethylsiloxane (PDMS from Sylgard 184, Dow Corning) modified with a solution of 80% ethoxylated polyethylenimine (PEIE, Sigma-Aldrich). The PDMS base and curing agent were mixed in a 10:1 ratio by weight, and 35  $\mu$ L of PEIE was added per 10 g of the PDMS mixture to reduce the Young's modulus and roughen the surface to increase adhesion by van der Waals force.<sup>[35]</sup> This mixture was degassed and poured into a mold to cure at 90 °C for 3 h.

To pattern electrodes, conductive pastes were applied through a laser-etched stencil mask (Metal Etch Services, San Marcos, CA) using a blade coating applicator (Gardco). Each electrode had a diameter of 3 mm, while the center-to-center distance of the inner to outer electrodes was 9 mm. The interconnects and electrodes were patterned via screen printing through metal etched stencil masks. The silver/silver chloride ink (E2414, Ecron) was mixed with Ecoflex-50 (Smooth On) at a 94:6 weight ratio to increase electrode stretchability. This ink was annealed at 90 °C for 5 min. The poly(3,4-ethylenedioxythiophene) polystyrene sulfonate ink was formulated with 1 g of screen-printable PEDOT:PSS mixed with 0.4 mL of ethylene glycol to increase electrode conductivity, 5  $\mu$ L of 4-dodecylbenzenesulfonic acid as a surfactant, and 40 mg 3-glycidoxypropyltrimethoxysilane as a crosslinker. This PEDOT:PSS ink was deposited through a second stencil mask to cover the ends of the Ag/AgCl traces and cured at 120 °C for 1 h. A layer of PDMS was deposited on top of the Ag/AgCl traces to encapsulate and isolate them from the skin. Thin wires were embedded in the encapsulation layer to connect the printed electrodes to the power supply and measurement equipment for stimulation.

**Inkjet-Printed Electrode Fabrication:** Inkjet-printed electrodes were fabricated as detailed in ref. [21]. Harima gold nanopaste ink was printed on polyethylene naphthalate substrates with 30  $\mu$ m drop spacing using a Dimatix Materials Printer (DMP-2800) to form the gold interconnects. Printed gold nanopaste ink was cured with a slow ramp annealing step (30–230 °C with 0.7 °C min<sup>-1</sup> ramp), followed by a constant temperature bake at 230 °C for 1 h. Vias were then laser-cut in a Teflon tape and the tape was placed on top of the printed gold electrodes to act as the encapsulation layer.

To test charge injection capacity, electrodes with or without PEDOT:PSS coated on top of the electrode ends were compared, and because of this test, Au was used for the exposed electrodes instead of Ag, since Ag would be oxidized in the presence of aqueous solutions or hydrogels when ES was applied. Nonetheless, if the Ag was covered by PEDOT:PSS, the oxidization issue would be negligible and not observed. To coat PEDOT:PSS on the electrodes, a Kapton tape was laser cut to be used as a mask for stencil printing, and placed on the electrode array with openings aligned to the electrode ends. PEDOT:PSS was then stencil-printed through this mask and annealed at 100 °C for 10 min. The Kapton tape was then gently peeled off from the Teflon surface, leaving the intact electrode array and encapsulation layer. To increase the adhesion of the arrays on wound sites, a double-sided tape was attached to the electrodes. Vias to the electrodes were formed by a laser cutter.

For impedance mapping, low impedance hydrogels were made with 10% w/v gelatin dissolved in phosphate buffered saline (PBS), and high impedance hydrogels were made with 10% w/v gelatin dissolved in distilled water. Gels were warmed to 37 °C and deposited side by side on a glass slide for impedance measurements.

**PVA Sponge Implant and Harvest:** Implantation of PVA sponges (PVA Unlimited, Warsaw, IN) was performed in 6- to 8-week-old male C57BL/6 mice as described in refs. [15,44]. PVA sponges were hydrated in phosphate buffered solution, autoclaved, and then aseptically implanted subcutaneously in the back of the mice. Briefly, hair was shaved from the back of the mouse, an incision made to lift the skin, and the PVA sponge placed subcutaneously, after which the incision was sutured closed.<sup>[44]</sup> Three days after sponge implantation, mice were electrically stimulated with constant-current square-wave pulses for 1 h. All mouse procedures were approved by the UCSD Institutional Animal Care and Use Committee. Sponges were removed after stimulation experiments and processed to wash out cells for flow cytometry analysis by collecting sponges in 1 mL sterile PBS; the sponge compressed gently to release cells for subsequent fixation, permeabilization, and flow cytometry analysis.

**Electrical Stimulation:** Each individual electrode was coated with a drop of conductive hydrogel (SignaGel, Parker Laboratories Inc.) with a pipette tip immediately before use. The gel layer ensured electrical contact between the mice skin and the electrodes. Mice with implanted PVA sponges were then anesthetized using isoflurane. Once the animals were not responsive, they were placed in nose cones for the stimulation procedure. The skin around the wound site was cleaned with isopropanol wipes. The electrode array was placed on the wound site, such that the central electrode was aligned on top of the implanted PVA sponge, while the outer ring of electrodes surrounded the wound area (Figure 1C). The electrode array was secured via surgical tape, with even pressure applied over the wound site to keep the array in place during the course of the stimulation. Sham mice underwent the same procedure but were not electrically stimulated, as the electrode arrays were disconnected from the power supply.

For mice subjected to electrical stimulation, the electrodes were connected to a Keithley 2400 Source Meter (Tektronix). Constant-current square-wave pulses of the desired frequency were programmed via custom software implemented in LabView (National Instruments). The central electrode was connected to ground, while the outer electrodes were all connected to the positive terminal of the power supply. Stimulation was applied for 1 h before the PVA sponge was harvested for further processing. The applied current was limited to a maximum of 600  $\mu$ A, and the voltage was limited to below 5 V. In the stretchable electrode design, the edge-to-edge distance between the center electrode and outer electrodes is 6 mm. Thus, the maximum electric field is 0.83 V mm<sup>-1</sup>. In the case of the inkjet-printed electrodes, since the distance between the outer ring and inner ring of electrodes is 5 mm, as shown in Figure S3, Supporting Information, the maximum electric field applied is 1 V mm<sup>-1</sup>.

**Immunostaining and Flow Cytometry:** Cells harvested from the PVA sponges were analyzed via flow cytometry. Harvested cells were fixed and permeabilized cells then labeled with CD45-VioGreen (130-110-803; Miltenyi Biotec, Bergisch Gladbach, Germany), CD11b-APC-Vio770 (130-109-288; Miltenyi Biotec), Ly6C-APC (130-102-341; Miltenyi Biotec), and either P-Erk (Cell Signaling, #14095) or P-Akt (Cell Signaling, #5315). For analysis of viability, a subset of the harvested cells was labeled with propidium iodide (130-093-233; Miltenyi Biotec) without fixing and permeabilization and analyzed via flow cytometry.

**Analysis:** Flow cytometry data was analyzed using FlowJo software (FlowJo LLC, Ashland, OR) and statistical analysis was performed in R. Statistical significance was determined by two-sided Mann-Whitney U-test with  $p \leq 0.05$ . The mean fluorescent intensity of each data point was normalized to the average of the sham data points for each particular experiment. The figures in this manuscript follow the convention for plotting flow cytometry data, for which the numerical values are not included on the axes.

## Supporting Information

Supporting Information is available from the Wiley Online Library or from the author.

## Acknowledgements

K.W. and U.P. contributed equally to this work. This work was supported by NextFlex Award#042299 and UC San Diego Medical Devices and Systems Initiative funded by the Electrical and Computer Engineering Department. Part of the work was performed at the San Diego Nanotechnology Infrastructure of UCSD, which is supported by NSF ECCS-1542148.

## Conflict of Interest

The authors declare no conflict of interest.

## Keywords

electrical stimulation, flexible electrodes, phosphorylation proteins, wound healing

Received: May 8, 2019

Revised: July 30, 2019

Published online:

- [1] M. Ochoa, R. Rahimi, B. Ziaie, *IEEE Rev. Biomed. Eng.* **2014**, 7, 73.
- [2] T. R. Dargaville, B. L. Farrugia, J. a. Broadbent, S. Pace, Z. Upton, N. H. Voelcker, *Biosens. Bioelectron.* **2013**, 41, 30.
- [3] S. L. Swisher, M. C. Lin, A. Liao, E. J. Leeflang, Y. Khan, F. J. Pavinatto, K. Mann, A. Naujokas, D. Young, S. Roy, M. R. Harrison, A. C. Arias, V. Subramanian, M. M. Maharbiz, *Nat. Commun.* **2015**, 6, 6575.
- [4] M. Zhao, *Semin. Cell Dev. Biol.* **2009**, 20, 674.
- [5] R. Nuccitelli, P. Nuccitelli, C. Li, S. Narsing, D. M. Pariser, K. Lui, *Wound Repair Regener.* **2011**, 19, 645.
- [6] S. Ud-Din, A. Bayat, *Healthcare* **2014**, 2, 445.
- [7] S. Ud-din, A. Sebastian, P. Giddings, J. Colthurst, S. Whiteside, *PLoS One* **2015**, 10, e0124502.
- [8] P. E. Houghton, *Chronic Wound Care Manag. Res.* **2017**, 4, 25.
- [9] J. Hunkler, A. de Mel, *J. Multidiscip. Healthcare* **2017**, 10, 179.
- [10] M. Ashrafi, T. Alonso-Rasgado, M. Baguneid, A. Bayat, *Vet. Dermatol.* **2016**, 27, 235.
- [11] G. Thakral, J. Lafontaine, B. Najafi, T. K. Talal, P. Kim, L. A. Lavery, *Diabetic Foot Ankle* **2013**, 4, 22081.
- [12] A. Sebastian, S. A. Iqbal, J. Colthurst, S. W. Volk, A. Bayat, *J. Invest. Dermatol.* **2015**, 135, 1166.
- [13] M. Zhao, B. Song, J. Pu, T. Wada, B. Reid, G. Tai, F. Wang, A. Guo, P. Walczysko, Y. Gu, T. Sasaki, A. Suzuki, J. V. Forrester, H. R. Bourne, P. N. Devreotes, C. D. McCaig, J. M. Penninger, *Nature* **2006**, 442, 457.
- [14] D. J. Cohen, W. J. Nelson, M. M. M. Maharbiz, W. James Nelson, M. M. M. Maharbiz, *Nat. Mater.* **2014**, 13, 409.
- [15] A. Baird, C. Deng, M. H. Eliceiri, F. Haghi, X. Dang, R. Coimbra, T. W. Costantini, B. E. Torbett, B. P. Eliceiri, *Wound Repair Regener.* **2016**, 24, 1004.
- [16] M. R. Major, V. W. Wong, E. R. Nelson, M. T. Longaker, G. C. Gurtner, *Plast. Reconstr. Surg.* **2015**, 135, 1489.
- [17] J. M. Daley, S. K. Brancato, A. A. Thomay, J. S. Reichner, J. E. Albina, *J. Leukocyte Biol.* **2010**, 87, 59.
- [18] S. Qin, R. A. Dorschner, I. Masini, O. Lavoie-Gagne, P. D. Stahl, T. W. Costantini, A. Baird, B. P. Eliceiri, *FASEB J.* **2019**, 33, 6129.
- [19] R. F. Diegelmann, W. J. Lindblad, I. K. Cohen, *J. Surg. Res.* **1986**, 40, 229.
- [20] K. Wang, U. Parekh, T. Pailla, H. Garudadi, V. Gilja, T. N. Ng, *Adv. Healthcare Mater.* **2017**, 6, 1700552.

- [21] Y. Khan, F. J. Pavinatto, M. C. Lin, A. Liao, S. L. Swisher, K. Mann, V. Subramanian, M. M. Maharbiz, A. C. Arias, *Adv. Funct. Mater.* **2016**, *26*, 1004.
- [22] S. Venkatraman, J. Hendricks, Z. A. King, A. J. Sereno, S. Richardson-Burns, D. Martin, J. M. Carmona, *IEEE Trans. Neural Syst. Rehabil. Eng.* **2011**, *19*, 307.
- [23] M. Ganji, A. Tanaka, V. Gilja, E. Halgren, S. A. Dayeh, *Adv. Funct. Mater.* **2017**, *27*, 1703019.
- [24] K. R. Schulz, E. A. Danna, P. O. Krutzik, G. P. Nolan, *Curr. Protoc. Immunol.* **2007**, *78*, 1.
- [25] J. V. Olsen, B. Blagoev, F. Gnani, B. Macek, C. Kumar, P. Mortensen, M. Mann, *Cell* **2006**, *127*, 635.
- [26] K. M. K. Rao, *J. Leukocyte Biol.* **2001**, *69*, 3.
- [27] S. X. Lu, O. Alpdogan, J. Lin, R. Balderas, R. Campos-Gonzalez, X. Wang, G.-J. Gao, D. Suh, C. King, M. Chow, O. M. Smith, V. M. Hubbard, J. L. Bautista, J. Cabrera-Perez, J. L. Zakrzewski, A. A. Kochman, A. Chow, G. Altan-Bonnet, M. R. M. van den Brink, *Blood* **2008**, *112*, 5254.
- [28] Y. D. Shaul, R. Seger, *BBA Mol. Cell Res.* **2007**, *1773*, 1213.
- [29] B. D. Manning, A. Toker, *Cell* **2017**, *169*, 381.
- [30] P. T. Hawkins, L. R. Stephens, *BBA Mol. Cell Biol. L.* **2015**, *1851*, 882.
- [31] M. C. Mendoza, E. E. Er, J. Blenis, *Trends Biochem. Sci.* **2011**, *36*, 320.
- [32] D. R. Merrill, M. Bikson, J. G. R. Jefferys, *J. Neurosci. Methods* **2005**, *141*, 171.
- [33] P. Minhas, V. Bansal, J. Patel, J. S. Ho, J. Diaz, A. Datta, M. Bikson, *J. Neurosci. Methods* **2010**, *190*, 188.
- [34] B. Reid, M. Zhao, *Adv. Wound Care* **2014**, *3*, 184.
- [35] S. H. Jeong, S. Zhang, K. Hjort, J. Hilborn, Z. Wu, *Adv. Mater.* **2016**, *28*, 5765.
- [36] A. Schander, T. Tesmann, S. Stokov, H. Stemmann, A. K. Kreiter, W. Lang, in *2016 38th Annual Int. Conf. of the IEEE Engineering in Medicine and Biology Society (EMBC)*, IEEE, Piscataway, NJ **2016**, pp. 6174–6177.
- [37] M. Ramuz, A. Hama, M. Huerta, J. Rivnay, P. Leleux, R. M. Owens, *Adv. Mater.* **2014**, *26*, 7083.
- [38] B. C. K. Tee, J. Ouyang, *Adv. Mater.* **2018**, *30*, 1802560.
- [39] Z. Wu, W. Yao, A. E. London, J. D. Azoulay, T. N. Ng, *ACS Appl. Mater. Interfaces* **2017**, *9*, 1654.
- [40] M. L. Thomas, *Annu Rev Immunol.* **1989**, *7*, 339.
- [41] T. Fukui, Y. Dai, K. Iwata, H. Kamo, H. Yamanaka, K. Obata, K. Kobayashi, S. Wang, X. Cui, S. Yoshiya, K. Noguchi, *Mol. Pain* **2007**, *3*, 1744.
- [42] Y. Wang, M. Rouabhia, Z. Zhang, *Biochim. Biophys. Acta, Gen. Subj.* **2016**, *1860*, 1551.
- [43] Y. Keshet, R. Seger, Humana Press, Totowa, NJ **2010**.
- [44] D. L. Deskins, S. Ardestani, P. P. Young, *J. Vis. Exp.* **2012**, *62*, e3885.